

RSC Advances



This is an *Accepted Manuscript*, which has been through the Royal Society of Chemistry peer review process and has been accepted for publication.

Accepted Manuscripts are published online shortly after acceptance, before technical editing, formatting and proof reading. Using this free service, authors can make their results available to the community, in citable form, before we publish the edited article. This *Accepted Manuscript* will be replaced by the edited, formatted and paginated article as soon as this is available.

You can find more information about *Accepted Manuscripts* in the [Information for Authors](#).

Please note that technical editing may introduce minor changes to the text and/or graphics, which may alter content. The journal's standard [Terms & Conditions](#) and the [Ethical guidelines](#) still apply. In no event shall the Royal Society of Chemistry be held responsible for any errors or omissions in this *Accepted Manuscript* or any consequences arising from the use of any information it contains.

Synthesis of polyurea-polyether nanoparticles via spontaneous nanoprecipitation.

Pietro Locatelli¹, Steve Wouters², Chris Lindsay², SLM Schroeder³, John H. Hobdell² and Alberto Saiani^{1*}

¹ School of Materials, The University of Manchester, M13 9PL Manchester, UK

² Huntsman Polyurethanes, Everslaan 45, 3078 Everberg, Belgium

³ School of Chemistry, The University of Manchester, Oxford Road, Manchester, M13 9PL, UK

* Corresponding author (E-mail: a.saiani@manchester.ac.uk)

Abstract:

We described here a novel synthetic route for the preparation of polyurea-polyether nanoparticles (PNP) that can be performed in a single solvent and which does not require the use of a preformed polymer. First a low molecular weight polyether-monoamine (poly(PO/EO)) is added drop wise to a solution of 4,4'-methylene-diphenylene isocyanate (4,4'-MDI). This leads to a solution of free 4,4'-MDI and low molecular weight 4,4'-MDI-functionalized poly(PO/EO). In a second stage a short diamine chain extender and additional 4,4'-MDI are added drop wise to the solution. This results in the formation of ABA polyether-polyurea-polyether block copolymer that spontaneous precipitates forming nanoparticles (PNPs). The PNPs were characterized using a variety of techniques including transmission electron microscopy (TEM), photon correlation spectroscopy (PCS) and X-ray photoelectron spectroscopy (XPS). The combined analysis suggests that the polyether-monoamine resides preferentially on the surface of the PNPs and has a role in their stabilization as well as in the stabilization of the resulting colloidal suspensions. The nature of the diamine chain extender was varied in order to explore its effect on the formation, properties and morphology of the nanoparticles. PNPs in the size range from 20 to 100 nm were obtained depending on the diamine used and the stability of the colloidal solution obtained was also found to be dependent on the diamine used.

Introduction

Polymer nanoparticles (PNPs) find applications in a wide variety of fields including electronics,¹ biotechnology² and environmental protection.³ Properties and morphology of PNPs can be controlled by varying the chemical structure and composition of the polymer as well as the preparation method used.⁴ There are two main routes for the preparation of PNPs: emulsion polymerization⁵ and precipitation of a preformed polymer.⁶ The latter encompasses a number of methods such as solvent evaporation, salting out, solvent displacement and nanoprecipitation.⁷ Emulsion polymerization typically involves the use of a monomer with low water solubility, a water soluble initiator and a surfactant to stabilize and homogenize the emulsion. The polymerization of PNPs is usually performed at high temperature and can take several hours to complete.⁸⁻¹⁰ The PNPs obtained through this route need to be purified to remove residual monomer, initiator and surfactant. Precipitation of a pre-formed polymer requires the use of three basic components: the polymer, the polymer solvent (e.g.: acetone, chloroform, ethanol or tetrahydrofuran) and the polymer non-solvent usually water.¹¹⁻¹³ The use of precipitation as a method to produce PNPs is limited by the large dilution that is required in order to obtain uniform particles.¹⁴ Indeed it has been shown that the formation of homogenous nanoparticles is confined to a small area of the composition map called the “Ouzo” region.¹⁵ Operating out of this region leads to unstable PNP suspensions resulting in the formation of large agglomerates. Nanoprecipitation is mainly used to produce polyesters nanoparticles for biomedical applications.¹⁶

Polyurethanes and polyureas have recently attracted significant attention for the production of nano- and micro-structured materials by spontaneous precipitation.¹⁷⁻²⁰ Polyureas in particular are good candidates due to their high rate of polymerization, synthetic versatility and superior hydrogen bonding capability²⁰⁻²². In this article we present a two-step synthetic strategy for the preparation of polyurea-polyether PNPs. This method does not require the use of initiator, surfactant or a pre-formed polymer and can be conducted in a single solvent. It exploits the high reactivity of amine and isocyanate groups and is based on a two stages solution polymerization of a polyurea-polyether

ABA block copolymers at room temperature followed by its spontaneous nano-precipitation into PNPs. Here we focus mainly on the morphological characterisation of the PNPs using a range of techniques including transmission electron microscopy (TEM), Fourier transform infrared (FTIR) spectroscopy, wide angle X-ray scattering (WAXS), X-ray photoelectron spectroscopy (XPS) and differential scanning calorimetry (DSC).

Materials and Methods

Materials: Commercially available 4,4'-methylenediphenylene isocyanate (4,4'-MDI - Suprasec MPR), polypropylene/polyethylene glycol (poly(PO/EO)) with a PO/EO ratio of $\sim 29/6$ and an average molecular weight of $M_w = 2005$ (Jeffamine M2005), 2,2'-Oxydi(ethyl-amine) (Jeffamine EDR104) and 1,4-Bis-(Aminomethyl)-Cyclohexane (Jeffamine XTA-808) were provided by Huntsman Polyurethanes. 4,4'-[1,3-Phenylenebis(1-Methyl-ethylidene)]Bisaniline and all other chemicals were bought from Sigma Aldrich. All the reactants were used as received.

Polyurea nanoparticles synthesis: 4,4' MDI, poly(PO/EO) monoamine and the diamines, were first dissolved separately in toluene (10 % wt.). The 4,4' MDI and bisaniline solutions were prepared at 100 °C and 40°C respectively to ensure full dissolution and then allowed to cool down to room temperature. The other solutions were prepared directly at room temperature.

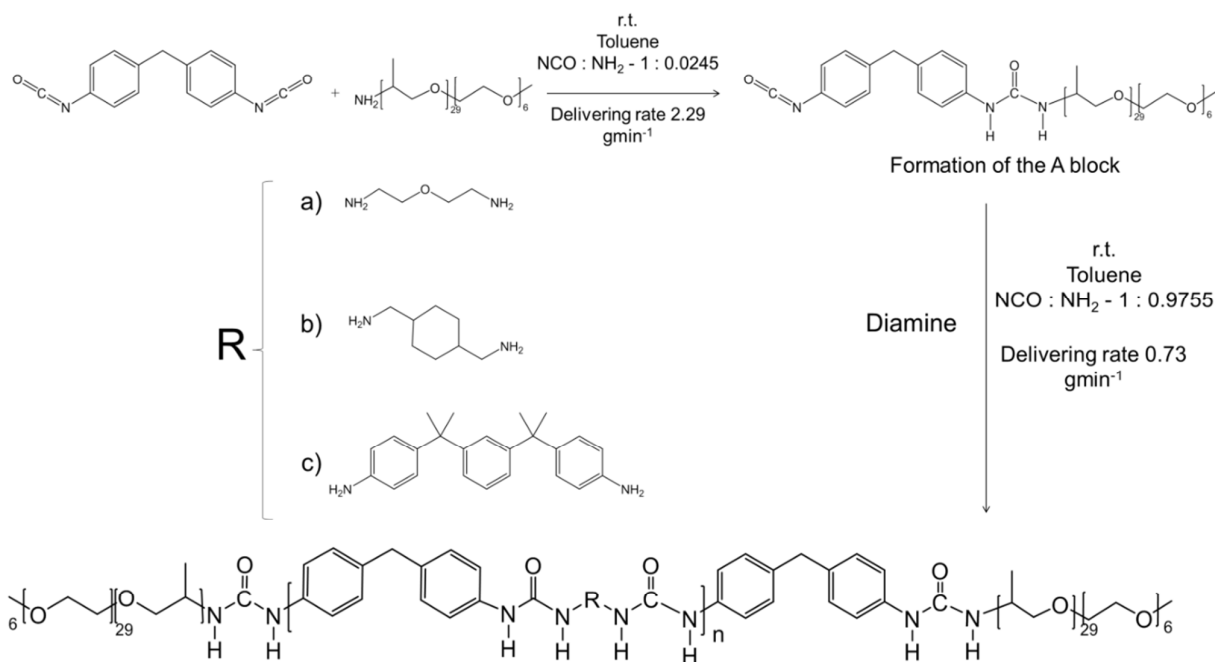


Figure 1: Scheme of the polyurea ABA block copolymer synthesis and chemical structure of the a) linear, b) cyclic and c) aromatic diamine chain extenders used.

The PNPs were synthesized via a two-step reaction (Figure 1). First the poly(PO/EO) solution was added drop wise to the 4,4' MDI solution under stirring conditions (overhead stirrer IKA Eurostar P.c.v. P1 33300.00) using a peristaltic pump (Watson Marlow 505S delivery rate 2.29 g min^{-1}). During the second step the desired diamine solution was added drop-wise (delivery rate 0.73 g min^{-1}) to the resulting solution which was stirred at all times. The reactant quantity and therefore the volumes of the solutions were calculated so as to have a 1:1 stoichiometric ratio between the NCO from the 4,4'-MDI and the NH_2 from the poly(PO/EO) monoamine and the diamines chain extenders. A diamine/monoamine molar NH_2 ratio of 40 (i.e.: diamine/monoamine molar ratio of 20) was used for this work. A slight excess of diamine was then added (0.1 % mol) to ensure complete reaction of the NCO groups. Assuming full conversion the theoretical weight average molecular weight of the 3 copolymers are: 14785, 18375 and 24604 g mol^{-1} for the linear, cyclic and aromatic chain extenders respectively. The polyurea PNPs suspensions obtained were stored at room temperature until needed. For ATR-FTIR and DSC measurements the PNPs were dried overnight and then for a further ~ 3 hours in a vacuum oven at room temperature.

Transmission electron microscope (TEM): Nanoparticles micrographs were taken using a FEI Tecnai 12 Biotwin operated at 100 kV. The suspensions were diluted in toluene to 0.005 % (wt.). One droplet was then placed on a copper grid (Holey carbon Film Agar Scientific) and allowed to dry. The images were analyzed using ImageJ free software. The average size of the particles was measured on ~ 150 randomly distributed and isolated PNPs except for the sample prepared using the aromatic diamine for which ~ 15 PNPs were used. The polydispersity index was calculated as the square of the ratio between the standard deviation on the average diameter.

Photon correlation spectroscopy (PCS): PCS measurements were performed using a BI-9000 Brookhaven light scattering apparatus (Brookhaven Instrument Corporation), fitted with a 20 mW He-Ne laser. The detector was set at a scattering angle of 90° . The PNP suspensions were diluted

in toluene to a final concentration of 0.05 % (wt.), sonicated for 10 minutes in an Elmasonic P sonicator (frequency: 37 kHz; power: 50 %) and then placed in a round glass cell.

Differential Scanning Calorimetry (DSC): DSC experiments were performed using a TA Q100 instrument calibrated with Zinc and Indium. Approximately 10 mg of sample was placed in a non-hermetic aluminium pan. Measurements were performed under dry N₂ atmosphere. The thermal protocol consisted in a heat/cool/heat cycle. The samples were brought to the start point of – 50 °C, heated up to 250 °C (1st heating cycle), cooled down (– 50 °C) and heated again (2nd heating cycle) to 250 °C. All measurements were performed at a rate of 20 °C min⁻¹. Data analysis was carried out using TA Universal Analysis software provided with the instrument. For the endotherms the transition temperature was taken at the minimum of the peak while for the glass transitions (T_g) the transition temperature was taken as the midpoint.

Attenuated Total Reflectance Fourier Transform Infrared Spectroscopy (ATR-FTIR): ATR-FTIR measurements were performed using a Thermo Nicolet 5700 spectrometer equipped with a Smart Orbit single bounce ATR attachment. FTIR spectra were collected in the 400 to 4000 cm⁻¹ spectral region with a sensitivity of 4 cm⁻¹ over 128 scans.

Atomic force microscopy (AFM): AFM topographic images were obtained using a Multimode AFM (Bruker nano) operating in peak force quantitative nano-mechanical mode. Images were acquired using the Nanoscope 8.13 software. The instrument was equipped with a commercial silicon tip (model TAP150A) with a nominal force constant of 5 N m⁻¹, a resonance frequency of 123-167 kHz and a tip radius > 15 nm. The nanoparticles were diluted in toluene or toluene and formic acid mixtures to a concentration of 0.02 % (wt.) and stirred for 24 h. The samples were then placed on a glass coverslip and allowed to dry. The coverslip was then mounted on a metal disc (diameter 12 mm) before imaging.

X-ray photoelectron spectroscopy (XPS). XP spectra were recorded with a Kratos Axis Ultra instrument employing a monochromatic Al K_{α} source (1486.69 eV). Survey spectra were measured with 80 eV pass energy in increments of 0.5 eV, with 100 ms dwell time per data point. High resolution spectra were measured within the spectral range of interest (ca. ± 20 eV around core level emission peaks) with 20 eV pass energy, 0.1 eV steps, and 100 ms dwell time for O 1s and C 1s and 200 ms for N 1s. Analysis of the data was carried out with Casa XPS software, using a linear background for curve-fitting and a GL(30) line shape (70 % Gaussian, 30 % Lorentzian).²³ An exponential tail GL(55)T(2) line shape was used for the O1s spectra as some intrinsic asymmetry was clearly visible toward higher binding energies (BE). Peak widths (full widths at half maximum) were allowed to vary within a range of 1.1 - 1.4 eV where multiple overlapping peaks were observed. In the following text and figure captions, when reporting binding energies for atoms in functional groups the atom referred to is underlined.

Results and Discussion

In Figure 2a) a schematic representation of the synthetic route used to prepare the PNPs is presented. First a low molecular weight polyether-monoamine, in our case polypropylene/polyethylene glycol (poly(PO/EO)), is added drop wise to a toluene solution of 4,4'-methylene-diphenylene isocyanate (4,4'-MDI). This leads to a solution of free 4,4'-MDI and low molecular weight 4,4'-MDI-functionalized poly(PO/EO). In a second stage a short diamine chain extender and additional 4,4'-MDI are added drop wise to the solution. The nature of the diamine chain extender was varied in order to explore its effect on the formation, properties and morphology of the nanoparticles. Three types of diamine were used (Figure 2c)): a linear etherdiamine: 2,2'-oxydi(ethyl-amine), a cyclic diamine: 1,4-bis-(aminomethyl)-cyclohexane and an aromatic diamine: 4,4'-[1,3-phenylenebis(1-methyl-ethylidene)] bisaniline.

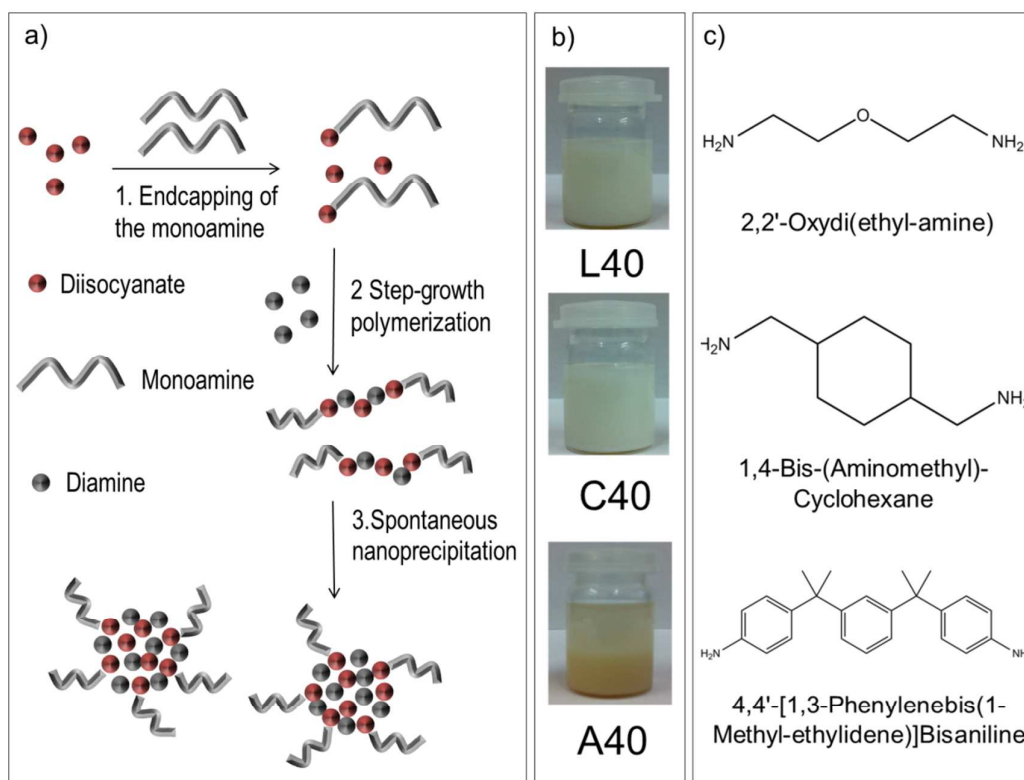


Figure 2: a) Schematic representation of the route used for the synthesis of the PNPs. b) Photograph of the dispersion obtained for each diamine chain extender c) Chemical structure of the diamine chain extenders used.

This second reaction results in the formation of an ABA block co-polymer (A block: poly(PO/EO) and B block: (4,4'-MDI-diamine)_n) that spontaneously precipitates into nanoparticles (see Figure 1 for chemical scheme). The chemical structure of the block copolymer can be controlled by varying the starting composition. Here we worked at a fixed diamine/monoamine NH₂ molar ratio of 40 (i.e.: diamine/monoamine molar ratio of 20). The final weight fraction of PNPs in suspension was 10 %.

As can be seen from Figure 2b the nature of the diamine used affects the stability of the colloidal suspension. For the sample prepared using the linear diamine (L40) a stable suspension was obtained while for samples prepared using the cyclic (C40) and the aromatic (A40) diamines unstable suspensions were obtained with A40 suspension being the less stable.

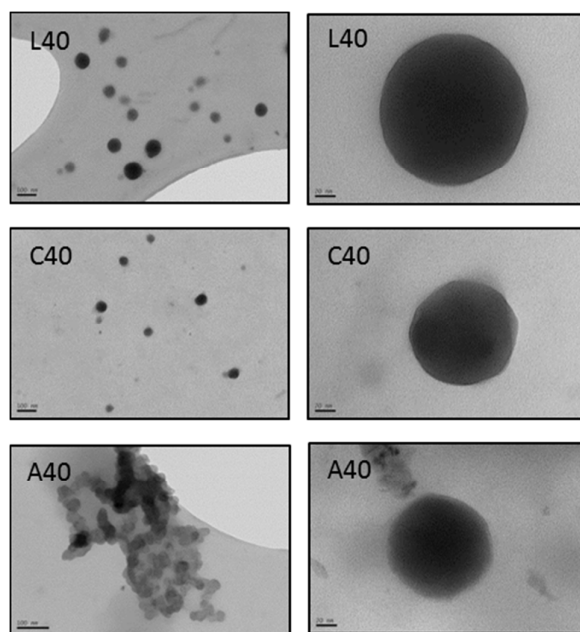


Figure 3: Transmission electron microscopy photograph of nanoparticles obtained with the linear (L40), cyclic (C40) and aromatic (A40) diamine chain extenders. (Scale bar: 100 nm left panels; 20 nm right panels).

The nanoparticles were visualized using TEM. As can be seen from Figure 3 for all three diamines spherical nanoparticles could be observed with sizes ranging from 20 to 150 nm. TEM

also confirmed the strong tendency for nanoparticles prepared using the aromatic diamine to aggregate indeed for the A40 sample large aggregates of nanoparticles were mainly observed with few isolated nanoparticles being visible. The sizes of the nanoparticles/aggregates were also estimated using photon correlation spectroscopy (PCS). It should be kept in mind that hydrodynamic diameters, d_H , are measured by PCS, which are typically 5-10 % larger than the actual physical size of the nanoparticles. In addition d_H measured will be affected by the presence of any PNP aggregates in the solution.

Sample	PCS		TEM	
	d_H /nm	PDI	d (σ)/nm	PDI
L40 (linear)	182 ± 1	0.22	87.7 (37.4)	0.18
C40 (cyclic)	300 ± 24	0.24	63.8 (24.9)	0.15
A40 (aromatic)	> 600	-	$\sim 60^*$	-

*diameter measured on less than 15 nanoparticles.

Table 1: Nanoparticles and aggregates size measured by TEM and PCS respectively. d_H : hydrodynamic diameter of the aggregates dispersed in toluene. d : average diameter of isolated PNPs estimated from TEM photographs (standard deviation in brackets). PDI: polydispersity index.

In Table 1 the average sizes measured by TEM and PCS are presented. The average diameters obtained by TEM for the isolated nanoparticles range from 60 nm for the A40 and C40 samples to 90 nm for the L40 sample. For the L40 sample the d_H obtained (~ 180 nm) suggests that although a stable suspension is obtained, low level of nanoparticles aggregation is still occurring in this sample. For the C40 sample a significantly larger d_H is obtained (~ 300 nm) although the TEM results suggest smaller particles are formed, clearly indicating that PNPs form large aggregates in this case, ultimately leading to an unstable suspension. For the A40 sample very strong aggregation was observed and the size of the aggregates could not be resolved using PCS. This is in agreement

with the visual observation which showed that this system formed the most unstable suspension.

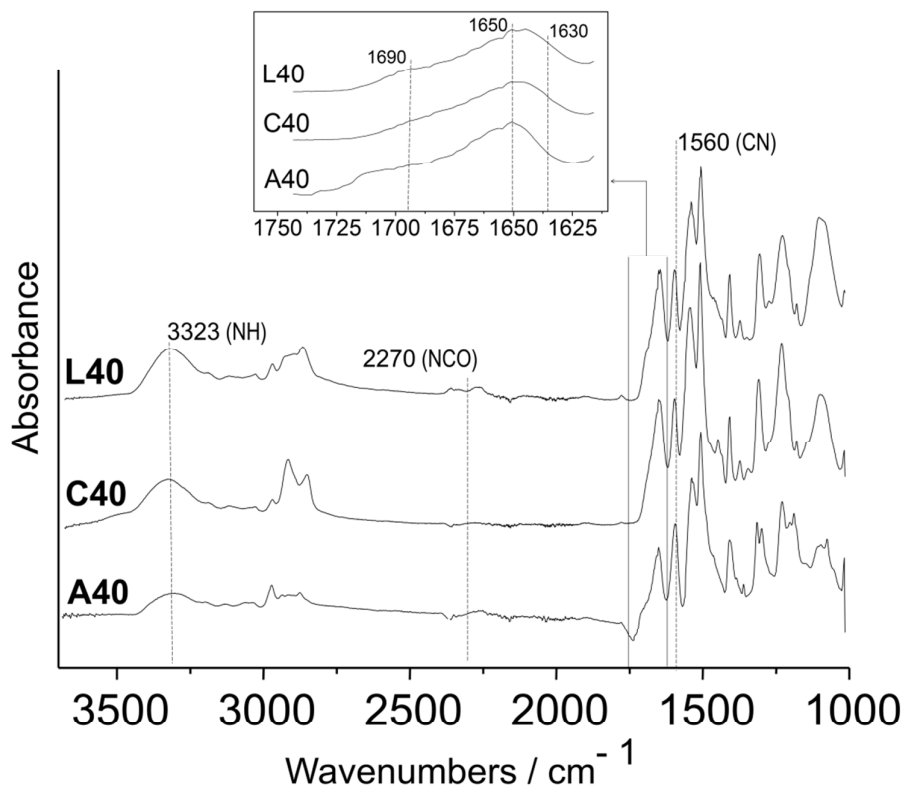


Figure 4: ATR-FTIR absorption spectra of polyurea PNPs obtained with the linear (L40), cyclic (C40) and aromatic (A40) chain extenders. Insert: expanded carbonyl vibration region.

In Figure 4 the ATR-FTIR spectra obtained for our three dried samples are presented. The absence of an absorption band corresponding to NCO groups at 2270 cm^{-1} suggests the full conversion of the isocyanates during the synthesis.¹⁷ In order to investigate the type of hydrogen bond formed within the nanoparticles the carbonyl region $1620 - 1700\text{ cm}^{-1}$ was examined more closely (insert Figure 4). Polyurea have the ability to form either linear (mono-dentate) or bi-dentate hydrogen bonds. Carbonyl groups involved in the latter type of hydrogen bonds absorb at lower wave number, typically $\sim 1630\text{ cm}^{-1}$, compared to groups involved in linear hydrogen bonds, $\sim 1650\text{ cm}^{-1}$, with free (non-bonded) carbonyl group absorbing at higher wave number, $\sim 1690\text{ cm}^{-1}$.²⁴ As can be seen from Figure 4 (insert) similar absorption spectra in the carbonyl

region were observed for all three samples: broad absorption band with a maximum centred around 1650 cm^{-1} . A shoulder at higher wave number corresponding to the absorption of free carbonyl can also be observed. These results suggest that linear hydrogen bonds mainly form. This type of hydrogen bonds are usually linked to the formation of poorly ordered structures in polyurea. The absence of well-defined crystalline structure in our nanoparticles was confirmed by WAXS (Figure ESI 1). In order to confirm that indeed the PNPs are kept together structurally by hydrogen bonds, formic acid was added to the dispersions to disrupt the hydrogen bonds.¹⁸ The addition of formic acid lead to the disruption of the PNPs and formation of polymer films / aggregates confirming the key role played by hydrogen bonding in the structural stabilisation of the PNPs (data not shown). It should also be noted that the PNPs formed could not be fully dissolved in any solvent without the addition of formic acid highlighting the strength of the hydrogen bonds in the core of the particles.

The nano-precipitation of the PNPs is thought to be mainly driven by the low solubility of the central (diamine-MDI)_n-blocks in toluene. Therefore we expect, as depicted in Figure 2a, the PNPs to have a morphology where the poly(PO/EO) resides at the surface of the nanoparticles. In order to confirm this point XPS was used to investigate the surface composition of the PNPs, as the probing depth of XPS in organic materials with Al K_α excitation is approximately 5 nm.²⁵ To carry out the XPS analysis, the following reference compounds corresponding to the central and side blocks of the ABA block co-polymer were also synthesised and analysed: (diamine-MDI)_n (sample names: L-MDI, C-MDI and A-MDI for the linear, cyclic and aromatic diamines respectively) and poly(PO/EO)-MDI-poly(PO/EO) (sample name: Mono-MDI).

In Figure 5 the survey XP spectra as well as high-resolution C 1s and O 1s spectra of the reference compounds are presented. The elemental composition of the reference compounds was found to be close to that expected from their known bulk compositions (Table ESI 1). These compounds were used to reference the binding energy scale for the analysis of the components fitted to the high resolution C 1s and O 1s spectra of the PNPs. The aliphatic C-H component of the C 1s spectra at 285.00 eV of the Mono-MDI sample was used for the calibration of the binding

energy scale as previously described.^{26,27}

The C 1s spectrum of the Mono-MDI sample is dominated by two peaks, corresponding to aliphatic $\underline{\text{C}}\text{-H}$ moieties at a binding energy of 285.0 eV and a $\underline{\text{C}}\text{-O}$ component at 286.6 eV. The $\underline{\text{C}}\text{-N}$ and $\text{C}=\text{C}$ contributions originating from the 4,4'-MDI are expected to be weak and to overlap with the strong $\underline{\text{C}}\text{-O}$ and $\underline{\text{C}}\text{-H}$ peaks, respectively. They could therefore not be resolved in the spectra. However, a small peak corresponding to the $\text{N}(\underline{\text{C}}=\text{O})\text{-N}$ urethane group is clearly seen at higher binding energy (288.8 eV) as it does not overlap with any other peak. This peak is clearly seen in isolation in all the reference compounds' as well as in all the PNP spectra, as will be seen below. It was therefore used to calibrate the binding energy scale of all the other samples. The O 1s spectrum is dominated by the peak originating from the $\text{C}\text{-}\underline{\text{O}}$ moiety and a small contribution from the $\text{N}(\underline{\text{C}}=\underline{\text{O}})\text{-N}$ group can be detected at lower binding energy. The binding energies obtained for all the reference compounds are summarized in Table 2.

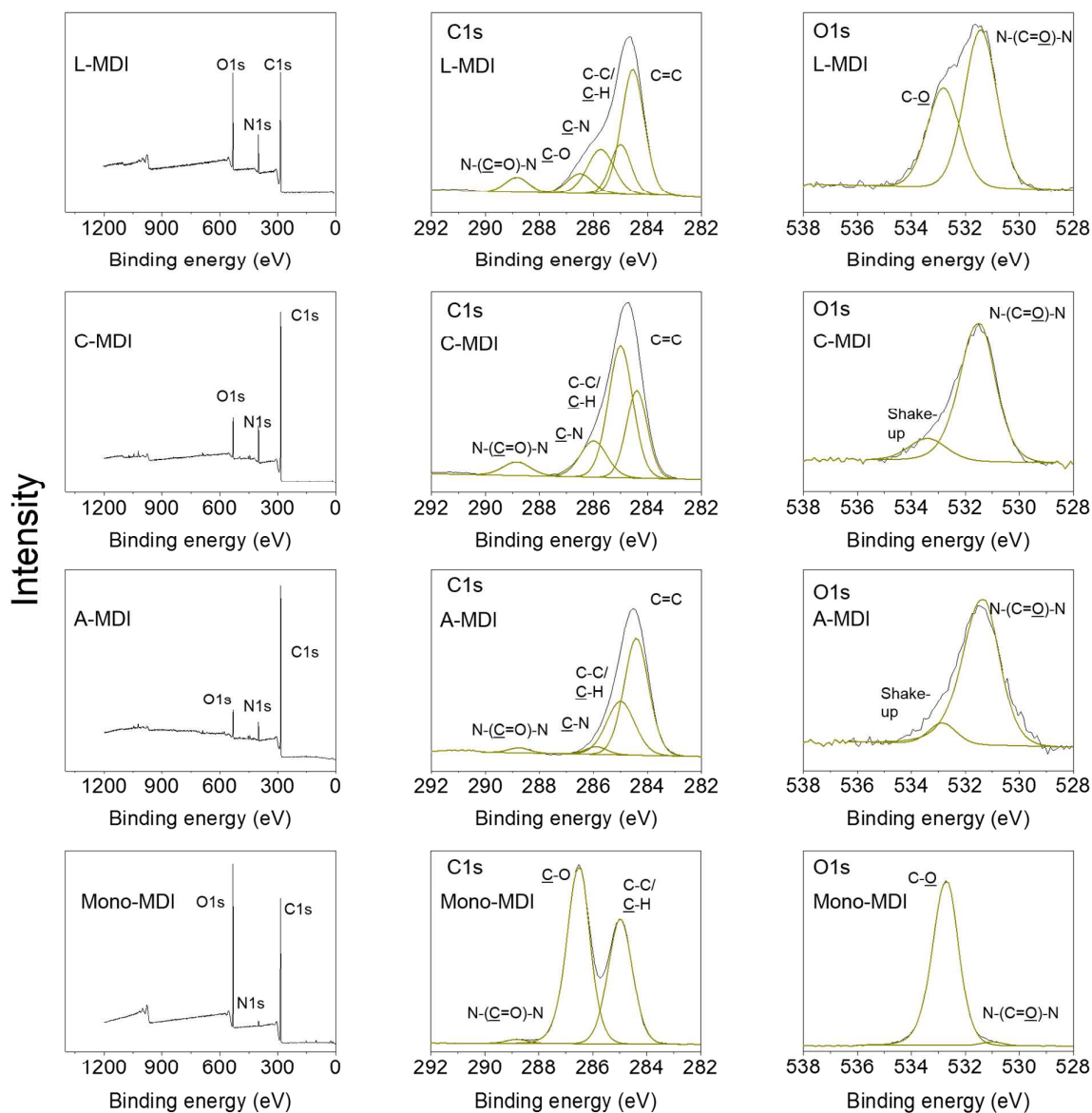


Figure 5: XPS elemental surveys (left) and C 1s (middle) and O 1s (right) spectra of reference compounds L-MDI, C-MDI, A-MDI and Mono-MDI and best fits (see text for more details).

For the A-MDI and C-MDI samples no $\underline{\text{C}}\text{-O}$ or C-O contributions are expected (see Figure 1). For these samples the C 1s spectra main peak is composed only of the three contributions corresponding to $\underline{\text{C}}\text{-N}$, $\text{C-C} / \underline{\text{C}}\text{-H}$ and $\text{C}=\text{C}$. In the case of the A-MDI sample the $\text{C}=\text{C}$ contribution is expected to be significantly stronger as this chain extender contains three vinyl rings. Indeed this is confirmed by the shift of the spectrum maximum towards lower binding energies (Figure 5). Both

spectra were fitted using three peaks with the C-C / C-H peak position fixed at 285.0 eV. As can be seen from Table 2 similar binding energies were obtained for $\underline{\text{C}}\text{-N}$ and C=C in both cases. As far as the O 1s spectra are concerned for both samples only an N-($\underline{\text{C}}\text{=O}$)-N contribution is expected, as no other oxygen is present (see Figure 1). In this case the spectra were fitted using two peaks, a main peak corresponding to N-($\underline{\text{C}}\text{=O}$)-N and a smaller peak at higher binding energies corresponding to the shake-up signal from the main peak.²⁸

Samples	C 1s					O 1s		
	$\underline{\text{C}}\text{-C}/\underline{\text{C}}\text{-H}$	C=C	$\underline{\text{C}}\text{-N}$	$\underline{\text{C}}\text{-O}$	N-($\underline{\text{C}}\text{=O}$)-N	$\underline{\text{C}}\text{-O}$	N-($\underline{\text{C}}\text{=O}$)-N	Shake-up
L-MDI	<i>285.0</i>	284.5	285.7	286.5	288.8	532.8	-	531.4
C-MDI	<i>285.0</i>	284.4	285.9		288.8	-	533.1	531.5
A-MDI	<i>285.0</i>	284.4	285.9		288.8	-	532.9	531.3
Mono-MDI	<i>285.0</i>	-		286.6	288.8	532.7	-	531.2

Table 2: C 1s and O 1s binding energies of the reference compounds (values in italics indicate fixed reference peak positions, as described in the text).

For the model compounds L-MDI $\underline{\text{C}}\text{-O}$ and $\underline{\text{C}}\text{-O}$ peaks are expected, as this diamine chain extender contains C-O species (see Figure 1). The C 1s spectrum main peak was therefore fitted using four peaks corresponding to $\underline{\text{C}}\text{-O}$, $\underline{\text{C}}\text{-N}$, C-C / $\underline{\text{C}}\text{-H}$ and C=C and the O 1s spectra using two peaks corresponding to $\underline{\text{C}}\text{-O}$ and N-($\underline{\text{C}}\text{=O}$)-N. The N-($\underline{\text{C}}\text{=O}$)-N shake-up peak was neglected as it overlaps with $\underline{\text{C}}\text{-O}$ and its contribution is small. Good agreement with the binding energies obtained for the reference compounds was obtained (Table 2).

We used the L-MDI sample to evaluate whether the O 1s spectra could be used to calculate the composition of samples quantitatively. Elemental compositions of 38.4 % for $\underline{\text{C}}\text{-O}$ and 61.6 % for N-($\underline{\text{C}}\text{=O}$)-N were obtained, in good agreement with the composition expected from the bulk stoichiometry of the samples, namely 33.3 % C-O and 66.7 % N-($\underline{\text{C}}\text{=O}$)-N, showing that the O 1s spectrum can indeed be used to estimate the elemental composition of the samples. In the C 1s

spectrum there is significant overlap between the peaks of the various components, so it could not be used for the determination of the elemental composition of the samples. All the composition results obtained from our fittings are summarised in Table ESI 2.

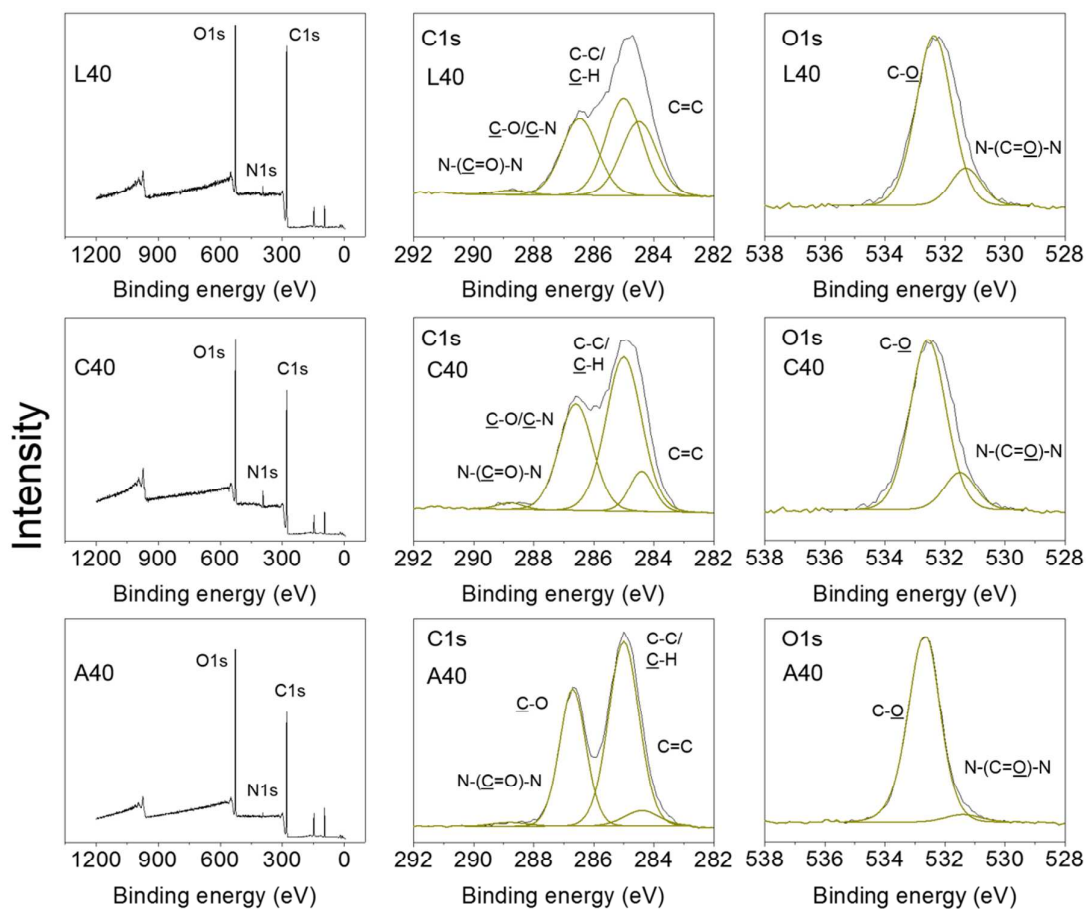


Figure 6: XPS elemental surveys (left) and C 1s (middle) and O 1s (right) spectra of PNP samples L40, C40 and A40 and best fits (see text for more details).

In Figure 6 survey spectra as well as the C 1s and O 1s spectra obtained for the three PNP samples are presented. In this case XPS indicated an elemental composition significantly different from the known bulk stoichiometry. In particular the nitrogen content was found to be significantly lower than expected; 2.3 % vs. 13.6 % for L40; 4.7 % vs. 12.0 % for C40; 0.4 % vs. 8.0 % for A40. As nitrogen is only present in the central (diamine-MDI)_n blocks of the copolymers these results

strongly suggest that the surface of the PNPs contains predominantly the poly(PO/EO) side block.

Samples	C 1s				O 1s	
	<u>C</u> -C/ <u>C</u> -H	C=C	<u>C</u> -N/ <u>C</u> -O	N-(<u>C</u> =O)-N	C- <u>O</u>	N-(C= <u>O</u>)-N
L40	38.8 %	29.4 %	30.4 %	1.6 %	83.8 %	16.2 %
<i>Theoretical values</i>	10.6 %	51.8 %	29.0 %	8.6 %	57.5 %	45.5 %
C40	53.6 %	9.6 %	35.2 %	1.6 %	81.7 %	18.3 %
<i>Theoretical values</i>	30.7 %	44.4 %	17.5 %	7.4 %	46 %	54 %
A40	56.7 %	5.4 %	36.5 %	1.4 %	95.9 %	4.1 %
<i>Theoretical values</i>	18.6 %	66 %	10.6 %	4.5 %	46.3 %	53.7 %

Table 3: Measured (from fitting of C 1s and O 1s spectra) and theoretical (from known sample bulk compositions) molar composition of the different species contributing to the C 1s and O 1s spectra of PNP samples (see text for more details)

The same fitting procedure as described for the reference compounds was used to fit the high resolution spectra of the PNP samples. However, for the C 1s spectra the C-O and C-N contributions were fitted using a *single* peak due to significant overlap between these two components. Also, for the O 1s spectra the N-(C=O)-N shake-up peak was neglected. Good agreement with the binding energy values obtained for the reference compounds is found (Table ESI 3). All the composition results obtained from our fittings are summarised in Table 3. The O 1s spectra were used to evaluate the elemental composition of the PNP surfaces. For the C40 and A40 samples the composition of the surface of the PNPs can be obtained directly, as C-O species are only present in the poly(PO/EO) side blocks while N-(C=O)-N species are only present in the (diamine-MDI)_n central blocks. For the L40 sample the diamine used also contains C-O species and therefore the C-O peaks originate from both the side and central blocks of the copolymers. In all three cases we assumed that the molar ratio between the MDI and the diamines in the central block

is constant and equal to the molar ratio used in the synthesis (1.05). The surface molar and mass compositions of the PNPs are summarised in Table 4. As can be seen the poly(PO/EO) resides mainly at the surface of the PNPs. This seems to be particularly marked for the A40 sample although this sample forms unstable suspensions and large PNPs aggregates are observed. The poly(PO/EO) is expected to play a role in the stabilisation of the PNPs and the resulting colloidal suspensions. These results suggest that the diamine used also strongly influences the stability of the colloidal suspension, in particular the more rigid the diamine the less stable the colloidal suspension. This points toward the key role played by the ability of the central block to fold during PNPs formation.

PNP surface		Poly(PE/EO)	MDI	Diamine
Compositions				
L(40)	molar fractions	12.1 %	45.0 %	42.9 %
	mass fractions	60.7 %	28.2 %	11.2 %
C(40)	molar fractions	11.6 %	45.3%	43.1 %
	mass fractions	57.0 %	27.9 %	15.1 %
A(40)	molar fractions	40.6 %	30.4 %	28.9 %
	mass fractions	82.3 %	7.7 %	10.1 %
Samples bulk molar composition		2.4 %	50 %	47.6 %

Table 4: Surface composition of the PNPs obtained from XP spectra fitting. Samples' bulk molar composition calculated from stoichiometry used for synthesis.

Next the thermal properties of the PNPs were investigated. First the glass transitions temperatures (T_g) and the associated heat capacity changes (ΔC_p) of the central and side blocks were measured by investigating the thermal properties of the reference compounds discussed above. The DSC graphs and the T_g s and ΔC_p s obtained are shown and reported in Figure ESI 2 and Table ESI 4 respectively. As expected the use of the cyclic and aromatic chain extenders result in higher

T_g s due to the rigidity imparted by these chain extenders to the central blocks (L-MDI: 102.6 °C ; C-MDI: 194.6 °C ; A-MDI: 204.7 °C)

In Figure 7 the DSC graphs obtained for the dried (1st heating) and melted (2nd heating) PNP samples are presented.

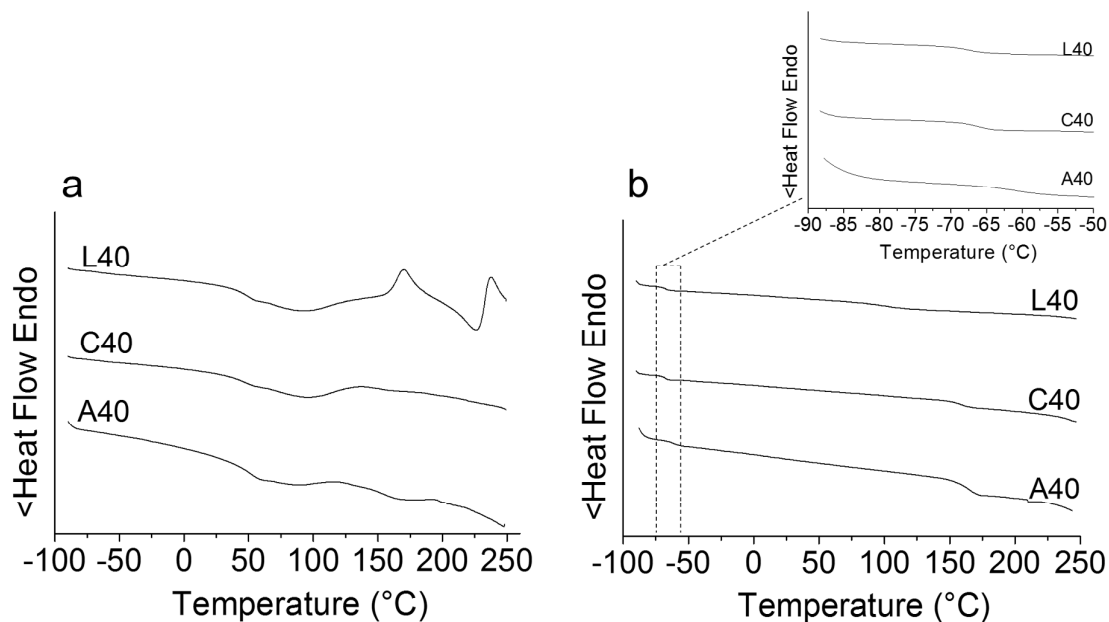


Figure 7: DSC graphs obtained at 10 °C min⁻¹ for the linear (L40), cyclic (C40) and aromatic (A40) samples. (a) 1st and (b) 2nd heating cycles respectively from -90 °C to 250 °C.

During the 1st heating cycle a T_g transition was observed for all three samples (Figure 7a) around 40 °C thought to correspond to the softening point of the PNPs. A broad endothermic transition is then observed again for all three samples around 100 °C which is believed to correspond to the release of residual toluene trapped in the core of the particles. Indeed the boiling temperature of toluene is 110 °C and TGA experiment (data not shown) reveal a ~ 5-7 % weight loss for all the samples between 50 and 110 °C. At higher temperatures for the L40 sample a typical behaviour of a semi-crystalline polymer quenched in an amorphous state below its T_g is observed. Just above the polymer's T_g a cold crystallisation exotherm is observed followed by a melting endotherm. For the

C40 and A40 samples small transitions are observed at higher temperatures thought to correspond to the T_g s of the polymers. As discussed above the poly(PO/EO) resides preferentially at the surface PNPs. The low softening point obtained ($< T_g$ of the (diamine-MDI)_n blocks) is thought to be due to the plasticising effect of the residual solvent and/or poly(PO/EO) trapped in the core of the PNPs during the nano-precipitation.

During the 2nd heating cycle i.e.: after melting the PNP the T_g s of the poly(PO/EO) and (diamine-MDI)_n blocks can clearly be seen for all three sample. This suggests that, as expected, these two blocks are highly incompatible and that upon melting and cooling phase separation occurs.²⁹⁻³¹ The detailed investigation of the thermal properties of these block copolymers is outside the scope of this article, nevertheless the thermodynamic incompatibility of the two blocks is also expected to contribute toward the poly(PO/EO) surface enrichment of the PNPs.

Conclusions

We have described a synthetic route for the preparation of polyurea-polyether PNPs that can be performed in a single solvent and which does not require the use of a preformed polymer. We showed that the type of diamine chain extender affects the size of the nanoparticles as well as the stability of the colloidal dispersions. Larger PNPs and a more stable dispersion were obtained for the linear diamine chain extender compared to cyclic and aromatic diamine chain extenders. The PNPs formed are believed to have a structure with the poly(PO/EO) residing mainly at the surface of the particles. This surface enrichment of the poly(PO/EO) component is thought to be due to the incompatibility of the two blocks as well as higher solubility of the polyether block in toluene.

Acknowledgments

The authors are grateful to Huntsman Polyurethanes and the EPSRC (University of Manchester, School of Materials DTA Fund) for funding this project. SLMS gratefully acknowledges financial support through EPSRC Critical Mass Grant EP/I013563/1.

References

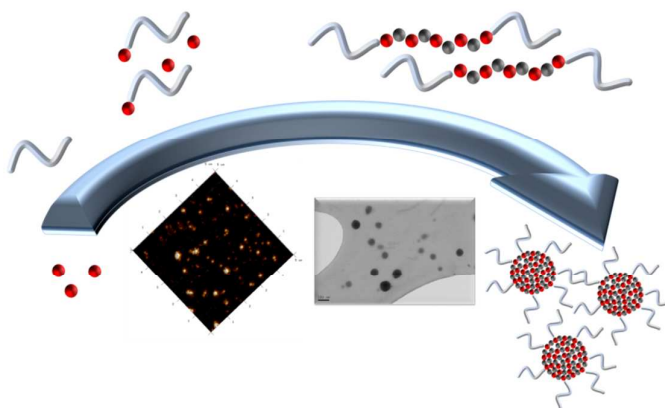
1. Schmid, G. n.; Schmid, G., *Nanoparticles : from theory to application*. Wiley-VCH: Weinheim, 2004; p x, 434.
2. Sudeep, P. K.; Page, Z.; Emrick, T., PEGylated silicon nanoparticles: synthesis and characterization. *Chem Commun (Camb)* **2008**, (46), 6126-7.
3. Zhang, Q. L.; Chuang, K. T., Adsorption of organic pollutants from effluents of a Kraft pulp mill on activated carbon and polymer resin. *Advances in Environmental Research* **2001**, 5, (3), 251-258.
4. Rao, J. P.; Geckeler, K. E., Polymer nanoparticles: Preparation techniques and size-control parameters. *Progress in Polymer Science* **2011**, 36, (7), 887-913.
5. Horn, D.; Rieger, J., Organic nanoparticles in the aqueous phase - theory, experiment, and use. *Angewandte Chemie-International Edition* **2001**, 40, (23), 4331-4361.
6. Soppimath, K. S.; Aminabhavi, T. M.; Kulkarni, A. R.; Rudzinski, W. E., Biodegradable polymeric nanoparticles as drug delivery devices. *Journal of Controlled Release* **2001**, 70, (1-2), 1-20.
7. Schubert, S.; Delaney, J. T.; Schubert, U. S., Nanoprecipitation and nanoformulation of polymers: from history to powerful possibilities beyond poly(lactic acid). *Soft Matter* **2011**, 7, (5), 1581-1588.
8. Tauer, K.; Deckwer, R.; Kuhn, I.; Schellenberg, C., A comprehensive experimental study of surfactant-free emulsion polymerization of styrene. *Colloid and Polymer Science* **1999**, 277, (7), 607-626.
9. Odian, G. G., *Principles of polymerization*. 4th ed.; Wiley-Interscience: Hoboken, N.J., 2004; p xxiv, 812.
10. Shi, L.; Shan, J.; Ju, Y.; Aikens, P.; Prud'homme, R. K., Nanoparticles as delivery vehicles for sunscreen agents. *Colloids and Surfaces A: Physicochemical and Engineering Aspects* **2012**, 396, 122-129.

11. Aschenbrenner, E.; Bley, K.; Koynov, K.; Makowski, M.; Kappl, M.; Landfester, K.; Weiss, C. K., Using the Polymeric Ouzo Effect for the Preparation of Polysaccharide-Based Nanoparticles. *Langmuir* **2013**, *29*, (28), 8845-8855.
12. Zhang, C.; Boucher, V. M.; Cangialosi, D.; Priestley, R. D., Mobility and glass transition temperature of polymer nanospheres. *Polymer* **2013**, *54*, (1), 230-235.
13. Zhang, C.; Chung, J. W.; Priestley, R. D., Dialysis Nanoprecipitation of Polystyrene Nanoparticles. *Macromolecular Rapid Communications* **2012**, *33*, (20), 1798–1803.
14. Aubry, J.; Ganachaud, F.; Addad, J. P. C.; Cabane, B., Nanoprecipitation of Polymethylmethacrylate by Solvent Shifting: 1. Boundaries. *Langmuir* **2009**, *25*, (4), 1970-1979.
15. Vitale, S. A.; Katz, J. L., Liquid droplet dispersions formed by homogeneous liquid-liquid nucleation: "The ouzo effect". *Langmuir* **2003**, *19*, (10), 4105-4110.
16. Hornig, S.; Heinze, T.; Becer, C. R.; Schubert, U. S., Synthetic polymeric nanoparticles by nanoprecipitation. *Journal of Materials Chemistry* **2009**, *19*, (23), 3838-3840.
17. Morral-Ruiz, G.; Solans, C.; Garcia, M. L.; Garcia-Celma, M. J., Formation of Pegylated Polyurethane and Lysine-Coated Polyurea Nanoparticles Obtained from O/W Nano-emulsions. *Langmuir* **2012**, *28*, (15), 6256-6264.
18. Foster, E. J.; Berda, E. B.; Meijer, E. W., Metastable Supramolecular Polymer Nanoparticles via Intramolecular Collapse of Single Polymer Chains. *Journal of the American Chemical Society* **2009**, *131*, (20), 6964-+.
19. Rosenbauer, E. M.; Landfester, K.; Musyanovych, A., Surface-Active Monomer as a Stabilizer for Polyurea Nanocapsules Synthesized via Interfacial Polyaddition in Inverse Miniemulsion. *Langmuir* **2009**, *25*, (20), 12084-12091.
20. Yang, Y.; Jiang, X.; Zhu, X.; Kong, X. Z., A facile pathway to polyurea nanofiber fabrication and polymer morphology control in copolymerization of oxydianiline and toluene diisocyanate in acetone. *Rsc Advances* **2015**, *5*, (10), 7426-7432.

21. Wagh, S. J.; Dhupal, S. S.; Suresh, A. K., An experimental study of polyurea membrane formation by interfacial polycondensation. *Journal of Membrane Science* **2009**, 328, (1-2), 246-256.
22. Xu, J.; Han, H.; Zhang, L.; Zhu, X.; Jiang, X.; Kong, X. Z., Preparation of highly uniform and crosslinked polyurea microspheres through precipitation copolymerization and their property and structure characterization. *Rsc Advances* **2014**, 4, (61), 32134-32141.
23. Fairley, N.; Carrick, A.; Walton, J., *The Casa cookbook*. Acolyte Science: Knutsford, 2005.
24. Coleman, M. M.; Sobkowiak, M.; Pehlert, G. J.; Painter, P. C.; Iqbal, T., Infrared temperature studies of a simple polyurea. *Macromolecular Chemistry and Physics* **1997**, 198, (1), 117-136.
25. Tanuma, S.; Powell, C. J.; Penn, D. R., Calculations of Electron Inelastic Mean Free Paths .5. Data for 14 Organic-Compounds over the 50-2000 Ev Range. *Surface and Interface Analysis* **1994**, 21, (3), 165-176.
26. Stevens, J. S.; de Luca, A. C.; Pelendritis, M.; Terenghi, G.; Downes, S.; Schroeder, S. L. M., Quantitative analysis of complex amino acids and RGD peptides by X-ray photoelectron spectroscopy (XPS). *Surface and Interface Analysis* **2013**, 45, (8), 1238-1246.
27. Stevens, J. S.; Schroeder, S. L. M., Quantitative analysis of saccharides by X-ray photoelectron spectroscopy. *Surface and Interface Analysis* **2009**, 41, (6), 453-462.
28. Briggs, D.; Beamson, G., *High Resolution XPS of Organic Polymers : Scienta ESCA300 Database*. Wiley: 1992; p [256]p.
29. Saiani, A.; Daunch, W. A.; Verbeke, H.; Leenslag, J.-W.; Higgins, J. S., Origin of Multiple Melting Endotherms in a High Hard Block Content Polyurethane: I. Thermodynamic Investigation. *Macromolecules* **2001**, 34, 9059-9068.
30. Saiani, A.; Novak, A.; Rodier, L.; Eeckhaut, G.; Leenslag, J. W.; Higgins, J. S., Origin of multiple melting endotherms in a high hard block content polyurethane: Effect of annealing temperature. *Macromolecules* **2007**, 40, (20), 7252-7262.

31. Saiani, A.; Rochas, C.; Eeckhaut, G.; Daunch, W. A.; Leenslag, J. W.; Higgins, J. S., Origin of multiple melting endotherms in a high hard block content polyurethane. 2. Structural investigation. *Macromolecules* **2004**, 37, (4), 1411-1421.

Graphical abstract:



Synthesis of polyurea-polyether core-shell nano-particles via spontaneous precipitation